


Multicolor ultralong phosphorescence from perovskite-like octahedral α -AlF₃

Received: 26 September 2021

Peisheng Cao¹, Haoyue Zheng² & Peng Wu^{1,2}  

Accepted: 22 September 2022

Published online: 29 September 2022

 Check for updates

Designing organic fluorescent and phosphorescent materials based on various core fluorophore has gained great attention, but it is unclear whether similar luminescent units exist for inorganic materials. Inspired by the BX₆ octahedral structure of luminescent metal halide perovskites (MHP), here we propose that the BX₆ octahedron may be a core structure for luminescent inorganic materials. In this regard, excitation-dependent color-tunable phosphorescence is discovered from α -AlF₃ featuring AlF₆ octahedron. Through further exploration of the BX₆ unit by altering the dimension and changing the center metal (B) and ligand (X), luminescence from KAlF₄, (NH₄)₃AlF₆, AlCl₃, Al(OH)₃, Ga₂O₃, InCl₃, and CdCl₂ are also discovered. The phosphorescence of α -AlF₃ can be ascribed to clusterization-triggered emission, i.e., weak through space interaction of the *n* electrons of F atoms bring close proximity in the AlF₆ octahedra (inter/intra). These discoveries will deepen the understanding and contribute to further development of BX₆ octahedron-based luminescent materials.

Luminescent materials are indispensable for our daily life, especially in lighting, displaying, and imaging-related applications^{1,2}. Therefore, luminescent materials design (either organic or inorganic) is of great importance and attracts great attention. It is widely accepted that luminescence from organic materials can be ascribed to their core structure in most cases (Fig. 1, together with the substituents), for example, fluorescent materials from xanthene^{3–7} and phosphorescent materials based on carbazole^{8–11}. Such core structure endow organic fluorophores with great flexibility and processability. While for inorganic luminescent materials, although structurally diverse and mostly acting as host materials for doping of transition- or rare-earth metal ions (e.g., ZnS¹² and SrAl₂O₄¹³), core structure as the light-emitting unit has seldom been reported and explored like organics. So, is there similar core structure for the luminescent inorganic materials?

All-inorganic metal halide perovskites (MHPs), a type of semiconductor materials with excellent photoelectric properties¹⁴, have been widely used in solar cells¹⁵, LED¹⁶, and thermoelectric modules¹⁷. The core structure of luminescent MHPs can be described as the BX₆ octahedron (Fig. 1), which is constituted by the central cation (B, hexacoordinated) and six halide ligands (X=Cl, Br, I). Normally, the BX₆ octahedron is organized in an all-corner-sharing 3D network. Due to the adjustable octahedral connectivity, a series of lower dimensional

metal halide-based luminescent perovskite derivatives have been reported¹⁸. On the other hand, the central cation and ligand halides could be altered, leading to tunable luminescence performance from 3D and lower dimension metal halides^{19,20}. Therefore, the BX₆ octahedron is an important structure for the luminescence of MHPs, but whether such unit can be generalized for other luminescent inorganic materials remains unexplored.

In this work, we find that inorganic materials constructed by the BX₆ octahedron exhibit interesting long-lived room temperature phosphorescence (RTP), i.e., the BX₆ octahedron may be regarded as a basic unit for the luminescent inorganic materials. For example, α -AlF₃, the material constructed by AlF₆ (the lightest BX₆ octahedron) with 3D perovskite-like structure²¹, shows color-tunable RTP (up to 7 s for the blue emission). When lowering the dimension of the AlF₆ octahedron, luminescence from KAlF₄ (2D) and (NH₄)₃AlF₆ (0D) is also discovered. Moreover, by changing B and X in the octahedral emissive unit of BX₆, luminescence from AlCl₃, Al(OH)₃, Ga₂O₃, InCl₃, and CdCl₂ are also obtained. Similar to BX₆ octahedron-based MHPs, the luminescence from AlF₃ exhibit typical self-trapped exciton (STE) emission. Besides, the octahedron also brings close proximity of F atoms, resulting in weak through-space interaction of the *n* electrons in F atoms for clusterization-triggered emission (CTE, recently found in *n* electron-rich

¹College of Chemistry, Sichuan University, Chengdu 610064, China. ²Analytical & Testing Center, Sichuan University, Chengdu 610064, China.

 e-mail: wupeng@scu.edu.cn

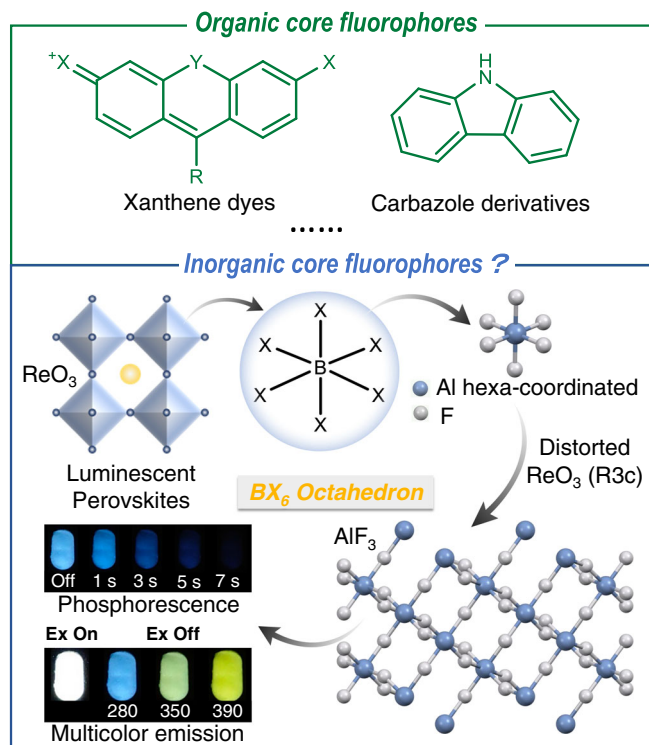


Fig. 1 | Schematic illustration of luminescent materials design. Inspired by the general luminescent material design based on organic core fluorophores and the widely investigated metal halide perovskites, here, we proposed BX_6 octahedral unit as inorganic luminescent core structure.

organics for excitation-dependent color-tunable phosphorescence^{22–24}). It should be noted that it is normally the heavy atoms that drives the formation of triplet and phosphorescence in inorganics (e.g., previous Al-based luminescent materials, Supplementary Table 1). However, $\alpha\text{-AlF}_3$ contains only light elements. Therefore, the discovery here is interesting for both organic and inorganic phosphors. In addition, the intriguing color-tunable phosphorescence without extra sophisticated molecular design can be explored for facile UV light detection with visible colored afterglow emission as readout.

Results

Luminescence of $\alpha\text{-AlF}_3$

To investigate the luminescent properties of the BX_6 octahedron, hexa-coordinated AlF_6 was chosen first. Considering its outermost electronic structure ($3s^23p^1$), aluminum is lightest atom to generate the octahedral structure. Meanwhile, F⁻ is the smallest anion²⁵ that can coordinate with Al^{3+} . The corner shared octahedra of AlF_6 results in the formation of three-dimensional network of $\alpha\text{-AlF}_3$ (Fig. 1). Normally, AlF_3 is used as the electrolyte regulator in the aluminum smelting industry for increasing the melting point and conductivity. However, its photophysical properties are rarely studied.

Here, we found AlF_3 exhibited exciting color-tunable luminescence at room temperature (Fig. 2a and Supplementary Fig. 3), irrespective of its origins (Supplementary Table 6 and Fig. 2). From the time-resolved emission spectra (TRES, Fig. 2b and Supplementary Fig. 11), the luminescence of $\alpha\text{-AlF}_3$ could be attributed to phosphorescence, with quantum yield (Φ_p) of ~4.22% and lifetime up to ~0.9 s ($\lambda_{\text{ex}} = 280$ nm, Fig. 2c). The room-temperature afterglow of $\alpha\text{-AlF}_3$ could last more than 7 s (naked eye observable), and the excitation-dependent blue to yellow afterglow could be visualized clearly after ceasing the excitation (Fig. 2d, Supplementary Figs. 12–13, and Supplementary Movies 1–3). The color-tunable emission was also clearly

revealed by the Commission Internationale de l'Éclairage (CIE) chromaticity coordinates (Fig. 2e). In addition, pure white light emission could be obtained (approaching CIE of 0.33, 0.33) when changing λ_{ex} from 270 nm to 390 nm (Fig. 2d and Supplementary Fig. 15).

To exclude the potential influence from trace impurities, direct synthesis of AlF_3 through exposing aluminum metal of the highest purity available to HF vapor was carried out. As expected, similar emission properties were also obtained (Supplementary Figs. 6–7), confirming that the luminescence was exactly from AlF_3 . Furthermore, the purchased and as-prepared samples were processed by calcination, ball milling, and acid-washing, and no appreciable change of the luminescence property was received (Supplementary Figs. 8–10).

Extending of the BX_6 octahedral luminescent unit

Since the 3D perovskite-like structure of $\alpha\text{-AlF}_3$ is constituted by the AlF_6 octahedron, the basic unit of BX_6 was further explored by adjusting the dimension of the octahedra (Fig. 3a). As shown in Figs. 3b and 3c, phosphorescence from KAlF_4 (2D, layers of corner-sharing AlF_6 octahedra and BCC coordinated K^+) and $(\text{NH}_4)_3\text{AlF}_6$ (0D, isolated AlF_6 octahedra surrounded by NH_3 ligands) was also collected (Supplementary Figs. 22 and 25), accompanied with similar excitation-dependent emission. The crystalline structure information (Supplementary Table 7) and XRD patterns confirmed that both KAlF_4 and $(\text{NH}_4)_3\text{AlF}_6$ were composed by the AlF_6 octahedral unit and belonged to 2D and 0D metal halides structures (Supplementary Fig. 20), respectively. It should be noted that lowering the dimension of the octahedra resulted in largely decreased phosphorescence intensity and shortened lifetime (Fig. 3c), indicating that the linkage of the AlF_6 octahedra also contributed to the observed phosphorescence.

Next, the ligand (X) of the BX_6 basic unit was changed with other halogens, namely AlCl_3 and AlBr_3 (Fig. 3a). As shown in Fig. 3d and Supplementary Fig. 23, AlCl_3 (cubic layered AlCl_6 octahedra) still exhibited appreciable long-lived phosphorescence (Fig. 3e and Supplementary Fig. 26 and Supplementary Movie 4). Through altering halide composition from F to Br, their emission spectra are readily tunable from blue to yellow (Insets of Fig. 3d), which was similar with the emission tunable perovskite materials through halide engineering²⁶. Although the outer space of Al is unable to accommodate six Br atoms to form stable hexadentate structure due to their relatively large atom radius discrepancy, AlBr_3 (tetrahedral) is still luminescent, but with significantly reduced intensity and shortened lifetime (Fig. 3d, 3e). When altering the ligand from F to O, phosphorescence from the AlO_6 (octahedral) derivatives ($\text{Al}(\text{OH})_3$ or Al_2O_3 , 2D sheets of edge sharing $\text{Al}(\text{OH})_6$ octahedra) was also collected (Fig. 3d and Supplementary Fig. 23).

Upon changing the metal center of BX_6 octahedral structure from Ga_2O_3 (mixture of GaO_6 octahedral and GaO_4 tetrahedral), InCl_3 (distorted InCl_6 octahedra in the 1D chains), and CdCl_2 (2D sheets of edge-sharing CdCl_6 octahedra) can be expected. Again, phosphorescence from these species was successfully collected (Fig. 3f and Fig. 3g, Supplementary Figs. 23 and 27, and Supplementary Movie 5 for Ga_2O_3 afterglow). It should be noted that there are diverse hexa-coordinate structures evolved from different bond angles (X–B–X), thus varied phosphorescence properties (excitation, emission, intensity, and lifetime, Fig. 3h)²⁷.

Luminescence mechanism of $\alpha\text{-AlF}_3$

The luminescence mechanism of the octahedral unit was investigated with the 3D network AlF_6 ($\alpha\text{-AlF}_3$). Compared with MHPs, $\alpha\text{-AlF}_3$ showed the 3D perovskite-like structure, but without the insertion of alkali metal cations. These cations only contribute to lattice stabilization and does not participate in the formation of the frontier molecule orbitals²⁸. The intrinsic emission of MHPs could be originated from free, bound and self-trapped excitons²⁹. Among them, self-trapped exciton (STE) emission is a well-accepted mechanism to account for

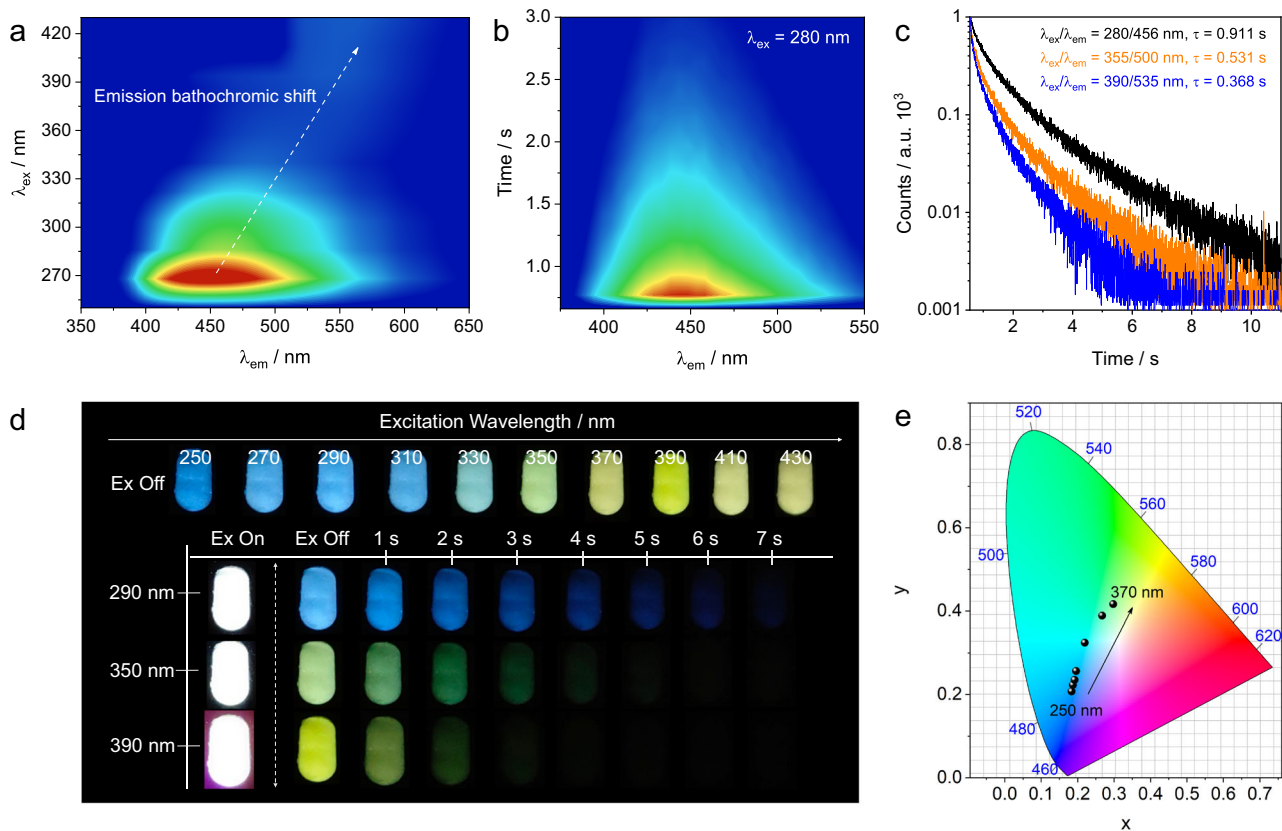


Fig. 2 | Luminescence properties of α -AIF₃ (calculated from AIF₃·3H₂O). **a** excitation- phosphorescence emission mapping of AIF₃ (delay time: 40 ms); **b** time-resolved emission spectra (TRES, $\lambda_{\text{ex}} = 280$ nm) of AIF₃; **c** lifetime decay profiles of phosphorescent emission excited at 280, 355, and 390 nm, respectively; **d** photographs taken under different excitation (250 to 430 nm) off and afterglow

emission images excited at 290, 350 and 390 nm, respectively (the excitation-dependent afterglow can be observed in the excitation range from 250 to 510 nm at room temperature condition); **e** CIE coordinates of AIF₃ phosphorescence under different excitation (250 to 370 nm).

the broadband and large-stokes shift emission^{30–33}. For α -AIF₃, similar broad-band excitation-dependent blue to yellow emission was emerged, with full width at half-maximum (FWHM) of 120 nm and Stokes shift up to -180 nm (Fig. 4a, emission spectra from $\lambda_{\text{ex}} = 250$ nm). In addition, a high energy narrow emission at 336 nm could be identified in the broad PL spectra (Fig. 4b), with lifetime of -2.05 ns (Fig. 4c). According to the previous reports^{34,35}, such emission could be ascribed to free excitons, which can be captured by the lattice distortion due to strong electron-phonon interaction in metal halides, resulting in the generation of STE.

The luminescence intensity of α -AIF₃ exhibited a linear dependence on the excitation power density (more than three orders of magnitude, Fig. 4d), indicating that the emission is originated from photogenerated exciton (self-trapped) rather than permanent defect, the latter of which would show saturated PL intensity upon increasing the excitation power density³⁶. Also, the emission band was not changed upon altering the excitation power density (Supplementary Fig. 16), further excluding the possibility of other emissive defects. Moreover, temperature-dependent phosphorescence spectra and cryogenic lifetime were collected (Supplementary Figs. 17, 18). The emission intensity was enhanced upon lowering the temperature (294 K \rightarrow 77 K), accompanied by a decrease in the FWHM (Fig. 4e), which was consistent with the characteristics of electron-lattice coupling³⁷. Therefore, all these above spectral features agreed well with STE.

On the other hand, although α -AIF₃ owns distorted 3D perovskite-like structure, its room-temperature phosphorescence exhibited interesting excitation-dependent feature. To further illustrate the mechanism, the transitions of AIF₃ was investigated through theoretical calculations. Considering that the BX₆ octahedra can be

luminescent in isolated, corner-shared, and distorted structures, a single unit of AIF₆ was calculated with the time-dependent density functional theory (TD-DFT)^{38,39}. The calculated excitation energy with the highest oscillator strength and the emission energy from the lowest triplet state (T_1) to the ground state (S_0) are 4.76 eV and 3.36 eV, respectively, indicating potential large Stokes shift. Next, the natural transition orbitals (NTO) were analyzed with Multiwfn⁴⁰. As shown in Fig. 5a and Supplementary Fig. 29, the transition with highest oscillator strength happened from the un-bonding n electron of F to the anti-bonding orbitals composed by the s orbital of Al and the p orbital of F. Meanwhile, such transition exhibited a typical $n \rightarrow \sigma^*$ character, which is consistent with the deep UV absorption of AIF₃. For phosphorescence transition ($T_1 \rightarrow S_0$), the frontier orbitals comprise F $2p$ (HOMO) as well as Al $3p$ and F $2p$ (LUMO). According to the selection rule for electronic spectra⁴¹, the electron transition of $p-p$ (similar to $f-f$ transition of lanthanides) orbitals is parity-forbidden, which is essential for the long-lived phosphorescence of AIF₃. For the other BX₆ octahedra, similar transitions ($n \rightarrow \sigma^*$) could also be identified and their $T_1 \rightarrow S_0$ transitions agreed well with experimental results (Supplementary Figs. 32–36).

Recently, a number of excitation-dependent color-tunable phosphors featuring $n \rightarrow \sigma^*$ transitions were reported, in which weak through-space interaction (TSI) was identified from the rich n electrons of the heteroatoms in the phosphors (cluster-induced emission, CIE)^{22–24}. Structurally, α -AIF₃ is a nonconjugated system without through-bond conjugation, but F atoms with n electrons are abundant to form corner sharing networks (Fig. 5b). Importantly, the distances between the adjacent F atoms in and between the AIF₆ octahedra (e.g., intra/inter: -2.544 and -2.549 Å; inter: -3.052 Å) generally fall in the van der Waals radii of F atom (1.47 Å)⁴². Therefore, there is possible

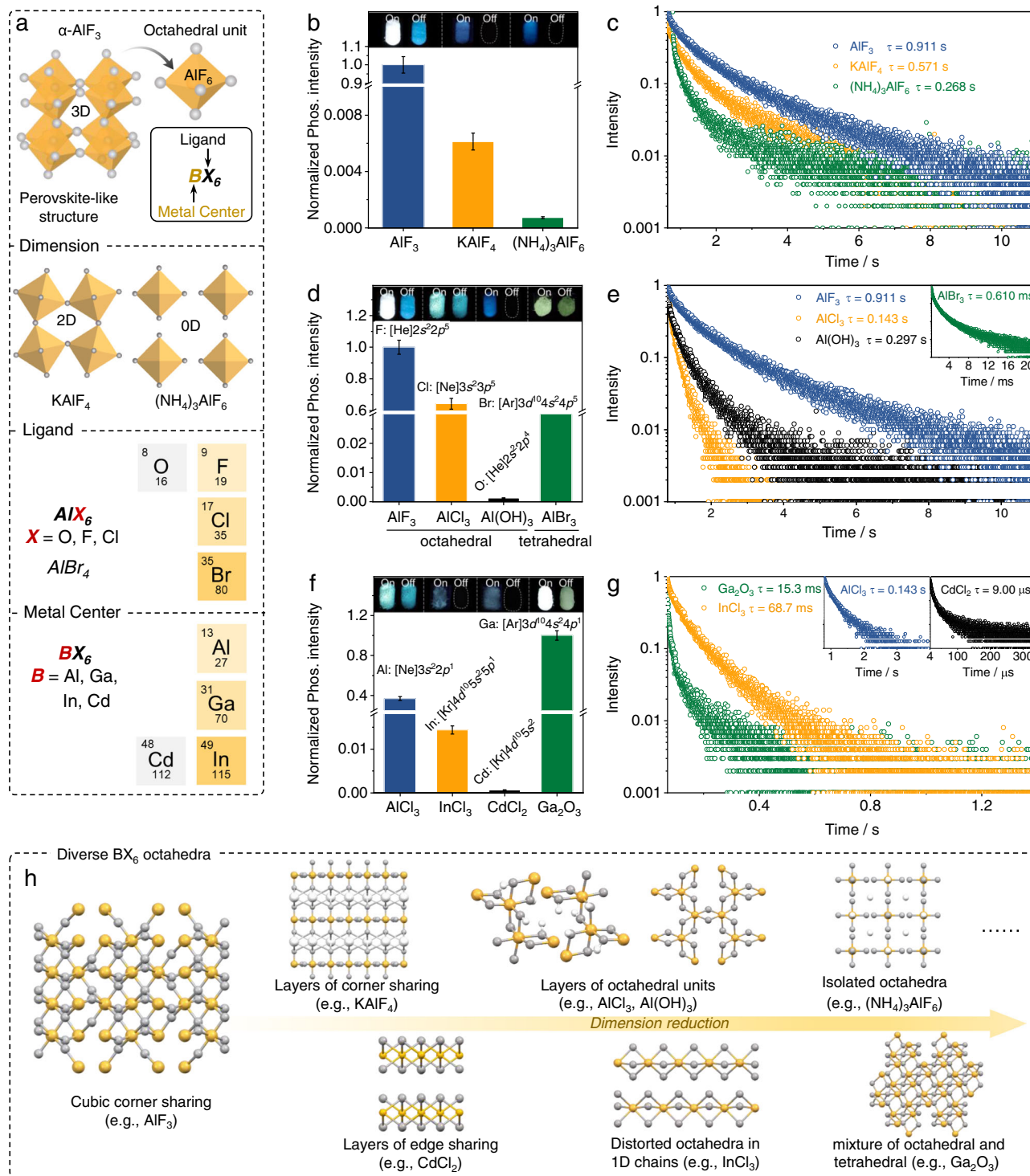


Fig. 3 | Investigation on the BX₆ octahedral luminescent unit. a, schematic diagram of chemical structure of AlF₃ and engineering of the octahedral basic unit; **b** and **c**, relative phosphorescence intensity and lifetime decay profiles ($\lambda_{ex} = 280$ nm) of the phosphorescence emission at 456, 480, 446 nm of AlF₃, KAIF₄, and (NH₄)₃AIF₆, respectively; **d**, **e**, relative phosphorescence intensity and lifetime decay profiles ($\lambda_{ex} = 280$ nm) of the phosphorescence emission at 456, 486, 450,

496 nm of AlF₃, AlCl₃, Al(OH)₃, and AlBr₃, respectively; **f**, **g**, relative phosphorescence intensity, and lifetime decay profiles ($\lambda_{ex} = 280$ nm) of the phosphorescence emission at 486, 468, 460, 500 nm of AlCl₃, InCl₃, CdCl₂, and Ga₂O₃, respectively; and **h**, summary of the diverse crystalline structures of the luminescent comprising BX₆ octahedra. Error bars represent standard deviation ($n = 3$).

van der Waals F...F interaction, thus leading to effective electron cloud overlap of the $n \rightarrow \sigma^*$ transition²³. It should be noted that F atoms also exist in NaF and KF, but no such phosphorescence could be found (Supplementary Fig. 24), further highlighting the importance of BX₆ octahedron.

Spectrally, the excitation spectra of α -AlF₃ contains two peaks, the short wavelength of which matches with its absorption, while those at longer wavelengths red shifted upon increasing the emission wavelengths (Fig. 5c). Besides, the excitation peaks at wavelength longer than the absorption were generally not detectable as a

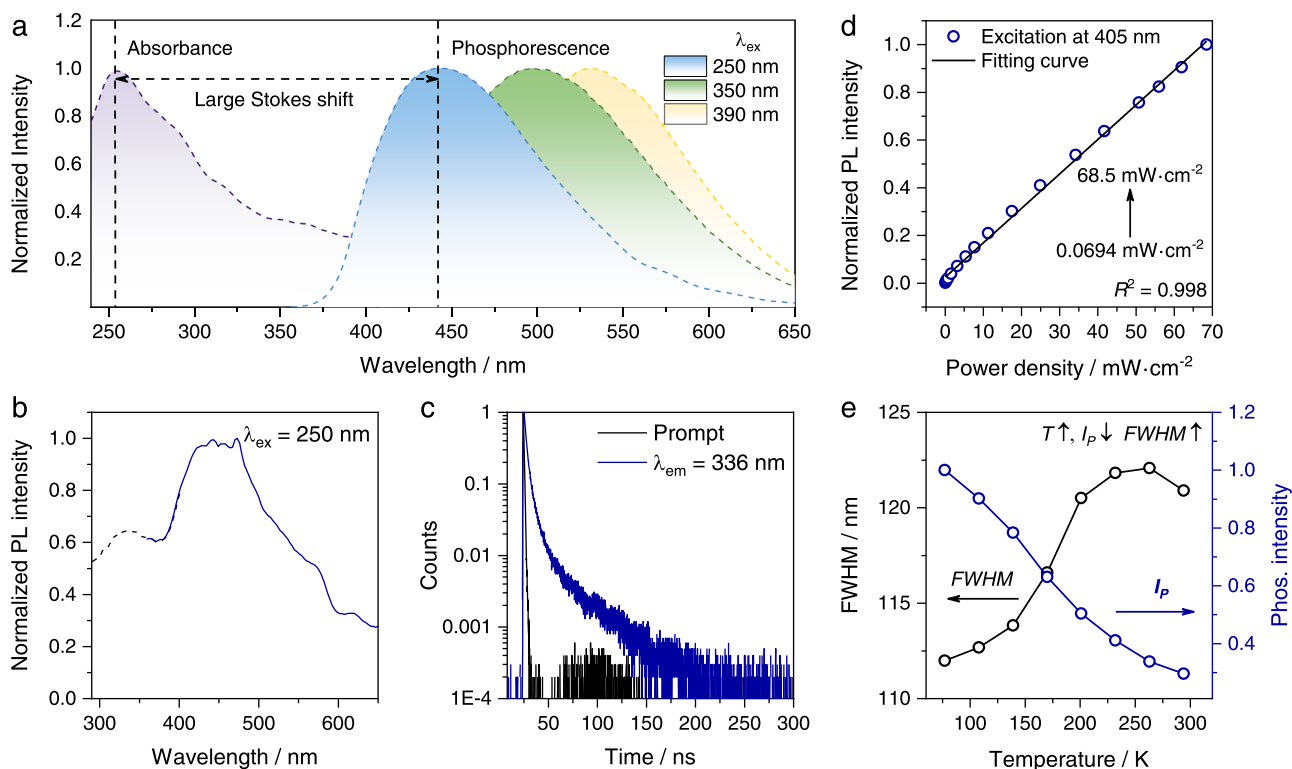


Fig. 4 | Investigation of the STE emission of AlF_3 . **a** Absorbance and phosphorescence spectra ($\lambda_{\text{ex}} = 280, 350,$ and 390 nm, respectively.); **b** Normalized PL spectra ($\lambda_{\text{ex}} = 250$ nm, the dotted line was measured without long pass filters, while the dashed line with 341 nm long pass filter placed at the emission exit); **c** lifetime of

AlF_3 monitored at 336 nm ($\lambda_{\text{ex}} = 280$ nm); **d** plot of PL intensity as a function of excitation power density ($\lambda_{\text{ex}} = 405$ nm); **e** plots of FWHM and intensity of phosphorescence as a function of temperature ($\lambda_{\text{ex}} = 280$ nm; delay time: 40 ms).

significant feature in the absorption spectra (Fig. 3a), which is also a typical sign of CTE. Moreover, as further calculated with the quantum mechanics and molecular mechanics (QM/MM) method, the energy gap decreased as increasing the number of AlF_6 octahedra (increasing the sizes of the clusters, Supplementary Fig. 30). Therefore, different clustering states may result in varied energy gaps (Fig. 5d), thereby excitation-dependent and color-tunable phosphorescence.

The weak interaction between AlF_6 octahedra in $\alpha\text{-AlF}_3$ was further investigated with Atoms in Molecules (AIM) analysis⁴³. As shown in Supplementary Fig. 31, in addition to traditional bond path in the octahedron (Al-F), there is also plenty of through-space interaction path (F...F interaction) as the AlF_6 octahedra system extended. Experimentally, upon high pressure treatment (900 MPa) to strengthen the weak intermolecular Van-der Waals interaction⁴⁴, the emission brightness of $\alpha\text{-AlF}_3$ was increased somewhat (Fig. 5e, Φ_p increase from -4.22% to -5.46%), while the multicolor emission profiles of $\alpha\text{-AlF}_3$ were not disturbed (Supplementary Fig. 19). Therefore, such interactions are expected to facilitate electron communications between the n electrons of F atoms and rigidify the system for efficient phosphorescence.

On the basis of the above analysis, similar excitation-dependent but decreased phosphorescence intensity from KAlF_4 and $(\text{NH}_4)_3\text{AlF}_6$ (and also other n electrons rich compounds featuring BX_6 octahedra, Fig. 3h) can thus be expected. Lowering the dimension of the AlF_6 octahedra from 3D corner-sharing ($\alpha\text{-AlF}_3$) to layered (KAlF_4) and isolated ($(\text{NH}_4)_3\text{AlF}_6$) would decrease the inter-octahedra F...F interaction, thus weakening the through-space interaction (Supplementary Fig. 21). Moreover, the 3D corner-sharing structure may also rigidify the AlF_6 octahedra, which is beneficial for stabilization of the excited triplet states. Therefore, compared with $\alpha\text{-AlF}_3$, lowering the dimension of the AlF_6 octahedra would result in sharply decreased

phosphorescence intensity and lifetime in KAlF_4 and $(\text{NH}_4)_3\text{AlF}_6$. For other BX_6 octahedron-containing materials, different phosphorescence performances would also be expected, due to their differences in B, X, and connection of the octahedra (Fig. 3h).

RTP of $\alpha\text{-AlF}_3$ for UV wavelength detection

Considering that the long-lived phosphorescence from AlF_3 is color-tunable in the visible range and excitation-dependent (particularly in the UV range), it was simply and conveniently explored for ultraviolet wavelength detection in a testing paper manner. As demonstrated in Fig. 6a, after mixed with Aloe vera gel for fixing, AlF_3 was coated on the filter paper. Upon UV irradiation, white luminescence from AlF_3 was excited (Fig. 6b). After ceasing of UV excitation, visible afterglow images could be obtained (Fig. 6c and Supplementary Movie 6). Notably, upon excited with UV light of different wavelengths, the afterglow emission varied from blue to orange, which could be further compared with standard color chart to confirm UV excitation wavelength (Fig. 6d and Fig. 6e). Such application provided a method for unknown UV wavelength detection and offered rapid and simple standard screening and testing of commercially UVA and UVB ultraviolet lamps available.

Discussion

In this work, perovskite-like octahedral BX_6 was proposed a basic unit for luminescent inorganic materials. In this regard, we found that $\alpha\text{-AlF}_3$ (constituted by vertex sharing AlF_6 octahedral unit) exhibited long-lived color-tunable phosphorescence emission, which could last up to 7 s and be observed by naked eyes. Besides, by lowering the dimension of the AlF_6 octahedron and changing B and X in the BX_6 octahedron, luminescence from KAlF_4 , $(\text{NH}_4)_3\text{AlF}_6$, AlCl_3 , $\text{Al}(\text{OH})_3$, Ga_2O_3 , InCl_3 , and CdCl_2 were also obtained. The phosphorescence of AlF_3 could also be explained with the well-accepted STE mechanism of perovskite BX_6

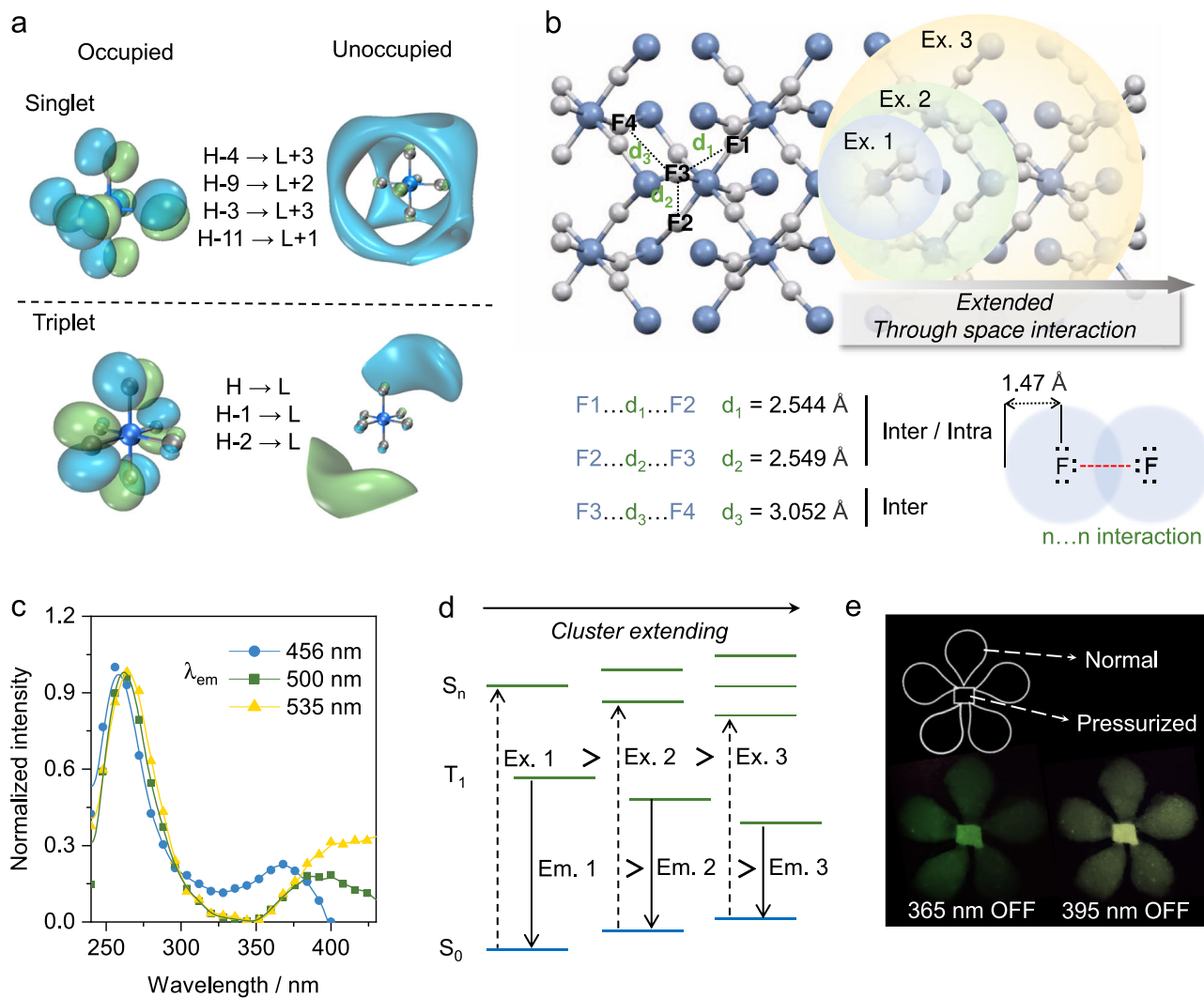


Fig. 5 | Investigation of the phosphorescence of AlF_3 . **a** the TD-DFT calculated isosurfaces of occupied and unoccupied orbitals of excited singlet state with maximum oscillator strength and lowest triplet excited state in AlF_6 octahedral unit. **b** structural analysis of $\alpha\text{-AlF}_3$ (crystalline structure from ICSD 68826).

c excitation spectra ($\lambda_{em} = 456, 500,$ and 535 nm, respectively.) of $\alpha\text{-AlF}_3$ **d** schematic energy level diagram of AlF_3 from one octahedron to network. **e** Photograph of AlF_3 afterglow with a flower pattern, consisting of untreated and pressure-treated $\alpha\text{-AlF}_3$, respectively.

octahedra, together with the clusterization-triggered emission of n electron-rich phosphors. Therefore, BX_6 octahedron may be a universal structure motif for inorganic luminescent materials (Fig. 7).

For a long time, it has been well-accepted that there are core structures for organic luminescent materials, and their general photophysical properties can thus be interpreted. For inorganic luminescent materials, such core structure remains elusive. Our results here indicated that the boundary between the above two may be somewhat vague. Inorganic AlF_3 (also AlCl_3 , Ga_2O_3 , and etc.), featured with perovskite-like octahedral BX_6 basic unit, can emit long-lived phosphorescence very much similar to CTE from non-conjugated organic luminophores²². Moreover, typical $n \rightarrow \sigma^*$ transition was found in the single unit of AlF_6 , which is also the typical character of CTE. Therefore, future development of luminescent materials integrating of both organic and inorganic luminescence mechanisms is expected to be appealing, particularly in MOFs containing both inorganic and organic units.

Last, in the long history of the afterglow phosphor family, the IIIA group elements contributed heavily (Supplementary Table 1, 2), particularly Al- and Ga-containing materials (e.g., the well-known $\text{SrAl}_2\text{O}_4:\text{Eu}^{2+}\text{-Dy}^{3+13}$ and $\text{ZnGa}_2\text{O}_4:\text{Cr}^{3+}$ ⁴⁵). However, the luminescence

center are mostly lanthanides or transition metal ions⁴⁶ (e.g., Mn^{2+} , and Cr^{3+}). Here, Al- and Ga-containing afterglow phosphors with ~4% QY (e.g., AlF_3 and Ga_2O_3) are discovered. Particularly, the luminescence is come from the Al- and Ga-involved octahedral unit, not the dopants. Therefore, there is still much room for the exciting IIIA group chemistry in luminescent materials design.

Methods

Preparation of AlF_3

AlF_3 was prepared through calcination of $\text{AlF}_3 \cdot 3\text{H}_2\text{O}$ (99.9%, Macklin) at 350 °C for 3 h. To eliminate potential organic impurities, other AlF_3 samples were also subjected to the same calcination process as above. In addition, direct synthesis of AlF_3 was carried out through exposing aluminum metal (Aladdin, 99.999%, the highest purity available) to HF vapor from hydrofluoric acid (Macklin, 49wt. % in H_2O , 99.99998%) for 3 h, followed by calcination at 350 °C for 3 h.

Phosphorescence measurements

Phosphorescence spectra were collected on HORIBA FluoroMax-4P with a delay time of 40 ms. For the temperature-dependent emission spectra, a model Optistat CF2 liquid nitrogen chamber

(Oxford Instruments) was used and coupled with the FluoroMax-4P spectrofluorometer. Phosphorescence lifetime and the time-resolved emission spectra (TRES) were collected on HORIBA FluoroLog-3 spectrofluorometer with 280, 355, and 390 nm spectralLED as the excitation sources, respectively. The absorption spectra of solid sample were measured on Shimadzu UV-3600 with an integrating sphere unit. The phosphorescence quantum yield (Φ_p) of samples were measured in an integrating sphere (IS80, Labsphere) using 2-fluorophenylboronic acid ($\Phi_p = 0.98\%^{47}$) as the reference ⁴⁸.

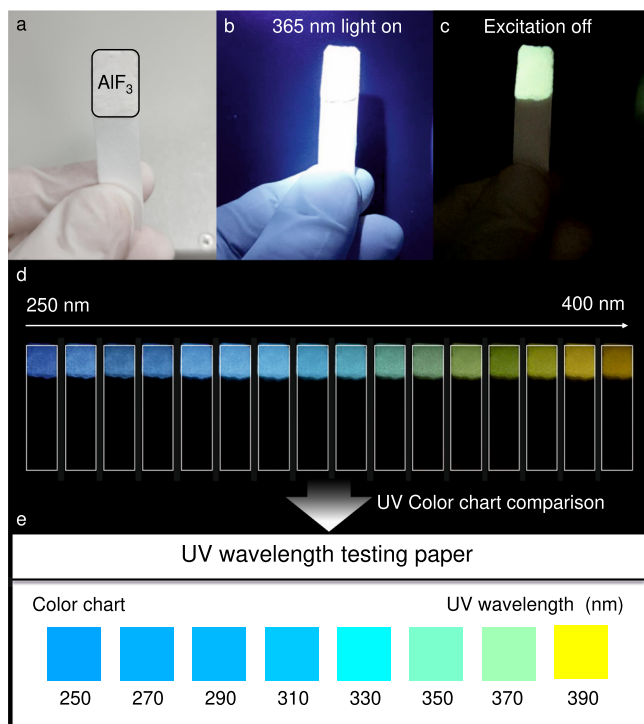


Fig. 6 | UV wavelength detection with AlF_3 -loaded testing paper. **a** illustration of the testing paper coated with AlF_3 ; **b** a beam of UV excitation irradiated on the testing paper; **c** AlF_3 -testing paper phosphorescence demonstration after ceasing 365 nm excitation; **d** multicolor phosphorescence from the AlF_3 -testing paper after ceasing a series of UV excitation; **e** color chart of UV wavelength testing paper.

Afterglow images

The samples were excited with light selected from the Xe lamp in the Fluolog-3 spectrofluorometer (250 to 510 nm)⁴⁸. The shutting of the excitation was controlled by instrumental software. The camera started to record video for 10 s after the excitation was turned off immediately.

Theoretical calculation

Theoretical calculations for the octahedral unit were performed on Orca program package (Revision 4.1.1). The ground states (S_0) were fully optimized by M062X with ma-def2-TZVP basis set. The excitation energies in the n -th singlet (S_n) and n -th triplet (T_n) states were obtained using the time-dependent density functional theory (TD-DFT) method based on an optimized molecular structure. In order to explore detailed excited state properties, NTO (Natural transition orbitals) analysis and hole-electron analysis method were further employed using Multiwfn program. For different cluster sizes of the AlF_6 octahedra, QM/MM method was applied to obtain optimized structure of isolated, layered and cubic corner sharing AlF_6 octahedra performed in the Gaussian 09 package⁴⁹. The central AlF_6 octahedra were treated at the (TD) M062X/6-31G+ (d,p) level, while the surrounding molecules were treated with universal force field (UFF).

For the weak interaction between AlF_6 octahedra, AIM analysis was carried out, which dictates the form of atoms in molecules and analyzes the topology of electron density. Typically, the results could be characterized by “critical points” of, namely bond (BCP), ring (RCP) and cage (CCP) critical points, representing the extreme points of electron density on the bond paths, centers of rings, and enclosed space formed by rings, respectively. It was further employed using Multiwfn program. The molecular orbitals (MO) and AIM models were all displayed using VMD.

UV wavelength testing paper

$\alpha\text{-AlF}_3$ was mixed with Aloe vera gel with mass ratio of -1: 1, followed by fixing on the filter paper to make the mixture evenly distributed and drying. For UV wavelength detection, the testing paper was first subjected to UV excitation for 5 seconds, then the afterglow images were either naked eye observed or photo taken with a camera.

Data availability

The data supporting the findings of this study are available within the paper and the Supplementary Information. Source data are provided with this paper.

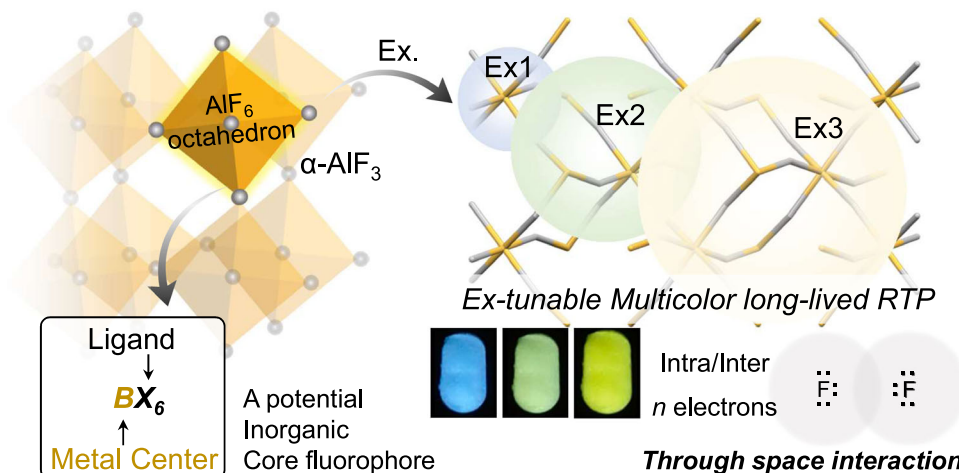


Fig. 7 | Summary on the BX_6 octahedra-based luminescence. Here, the luminescence mechanism of perovskite-like $\alpha\text{-AlF}_3$ (and also others) was ascribed to

clusterization-triggered emission of n electron-rich AlF_6 octahedrons, thus exhibiting excitation-tunable multicolor long-lived RTP.

References

- O'Hara, P. B., Engelson, C. & St Peter, W. Turning on the light: Lessons from luminescence. *J. Chem. Edu.* **82**, 49–52 (2005).
- Xu, J. & Tanabe, S. Persistent luminescence instead of phosphorescence: History, mechanism, and perspective. *J. Lumines* **205**, 581–620 (2019).
- Chen, X. Q., Pradhan, T., Wang, F., Kim, J. S. & Yoon, J. Fluorescent chemosensors based on spiroring-opening of Xanthenes and related derivatives. *Chem. Rev.* **112**, 1910–1956 (2012).
- Luo, X. et al. A diversity-oriented rhodamine library for wide-spectrum bactericidal agents with low inducible resistance against resistant pathogens. *Nat. Commun.* **10**, 258 (2019).
- Beija, M., Afonso, C. A. M. & Martinho, J. M. G. Synthesis and applications of Rhodamine derivatives as fluorescent probes. *Chem. Soc. Rev.* **38**, 2410–2433 (2009).
- Grimm, J. B. et al. A general method to improve fluorophores for live-cell and single-molecule microscopy. *Nat. Methods* **12**, 244–250 (2015).
- Wang, Y. et al. Halo-Fluorescein for photodynamic bacteria inactivation in extremely acidic conditions. *Nat. Commun.* **12**, 526 (2021).
- Jain, K. et al. Density functional investigation and some optical experiments on dye-sensitized quantum dots. *Phys. Chem. Chem. Phys.* **17**, 28683–28696 (2015).
- Chen, C. et al. Carbazole isomers induce ultralong organic phosphorescence. *Nat. Mater.* **20**, 175–180 (2021).
- Yang, Z. Y. et al. Intermolecular electronic coupling of organic units for efficient persistent room-temperature phosphorescence. *Angew. Chem. Int. Ed.* **55**, 2181–2185 (2016).
- Jin, J. B. et al. Thermally activated triplet exciton release for highly efficient tri-mode organic afterglow. *Nat. Commun.* **11**, 842 (2020).
- Wu, P. & Yan, X.-P. Doped quantum dots for chemo/biosensing and bioimaging. *Chem. Soc. Rev.* **42**, 5489–5521 (2013).
- Matsuzawa, T., Aoki, Y., Takeuchi, N. & Murayama, Y. A New long phosphorescent phosphor with high brightness, SrAl₂O₄:Eu²⁺,Dy³⁺. *J. Electrochem. Soc.* **143**, 2670–2673 (1996).
- Fu, Y. et al. Metal halide perovskite nanostructures for optoelectronic applications and the study of physical properties. *Nat. Rev. Mater.* **4**, 169–188 (2019).
- Tai, Q., Tang, K.-C. & Yan, F. Recent progress of inorganic perovskite solar cells. *Energy Environ. Sci.* **12**, 2375–2405 (2019).
- Lu, M. et al. Metal halide perovskite light-emitting devices: promising technology for next-generation displays. *Adv. Funct. Mater.* **29**, 1902008 (2019).
- Haque, M. A., Kee, S., Villalva, D. R., Ong, W.-L. & Baran, D. Halide perovskites: thermal transport and prospects for thermoelectricity. *Adv. Sci.* **7**, 1903389 (2020).
- Chen, P. et al. Progress and perspective in low-dimensional metal halide perovskites for optoelectronic applications. *Sol. RRL* **2**, 1700186 (2018).
- Li, M., Molochev, M. S., Zhao, J. & Xia, Z. Optical functional units in zero-dimensional metal halides as a paradigm of tunable photoluminescence and multicomponent chromophores. *Adv. Opt. Mater.* **8**, 1902114 (2020).
- Benin, B. M. et al. Highly emissive self-trapped excitons in fully inorganic zero-dimensional tin halides. *Angew. Chem., Int. Ed.* **57**, 11329–11333 (2018).
- Krahl, T. & Kernitz, E. Aluminium fluoride—the strongest solid Lewis acid: structure and reactivity. *Catal. Sci. Technol.* **7**, 773–796 (2017).
- Zhang, H. et al. Clusterization-triggered emission: Uncommon luminescence from common materials. *Mater. Today* **32**, 275–292 (2020).
- Tang, S. et al. Nonconventional luminophores: characteristics, advancements and perspectives. *Chem. Soc. Rev.* **50**, 12616–12655 (2021).
- Zhang, H. & Tang, B. Z. Through-space interactions in clusteroluminescence. *JACS Au* **1**, 1805–1814 (2021).
- Goesten, M. G., Hoffmann, R., Bickelhaupt, F. M. & Hensen, E. J. M. Eight-coordinate fluoride in a silicate double-four-ring. *Proc. Natl Acad. Sci.* **114**, 828 (2017).
- Protesescu, L. et al. Nanocrystals of cesium lead halide perovskites (CsPbX₃, X = Cl, Br, and I): Novel optoelectronic materials showing bright emission with wide color gamut. *Nano Lett.* **15**, 3692–3696 (2015).
- Filip, M. R., Eperon, G. E., Snaith, H. J. & Giustino, F. Steric engineering of metal-halide perovskites with tunable optical band gaps. *Nat. Commun.* **5**, 5757 (2014).
- Meloni, S., Palermo, G., Ashari-Astani, N., Grätzel, M. & Rothlisberger, U. Valence and conduction band tuning in halide perovskites for solar cell applications. *J. Mater. Chem. A* **4**, 15997–16002 (2016).
- Smith, M. D., Connor, B. A. & Karunadasa, H. I. Tuning the luminescence of layered halide perovskites. *Chem. Rev.* **119**, 3104–3139 (2019).
- Li, S., Luo, J., Liu, J. & Tang, J. Self-trapped excitons in all-inorganic halide perovskites: fundamentals, status, and potential applications. *J. Phys. Chem. Lett.* **10**, 1999–2007 (2019).
- Smith, M. D. & Karunadasa, H. I. White-light emission from layered halide perovskites. *Acc. Chem. Res.* **51**, 619–627 (2018).
- Zhou, L. et al. A highly red-emissive lead-free indium-based perovskite single crystal for sensitive water detection. *Angew. Chem., Int. Ed.* **58**, 5277–5281 (2019).
- Guo, Q., Zhao, X., Song, B., Luo, J. & Tang, J. Light emission of self-trapped excitons in inorganic metal halides for optoelectronic applications. *Adv. Mater.* <https://doi.org/10.1002/adma.202201008> (2022).
- Yuan, Z. et al. One-dimensional organic lead halide perovskites with efficient bluish white-light emission. *Nat. Commun.* **8**, 14051 (2017).
- Smith, M. D., Jaffe, A., Dohner, E. R., Lindenberg, A. M. & Karunadasa, H. I. Structural origins of broadband emission from layered Pb–Br hybrid perovskites. *Chem. Sci.* **8**, 4497–4504 (2017).
- Wu, G. et al. A one-dimensional organic lead chloride hybrid with excitation-dependent broadband emissions. *ACS Energy Lett.* **3**, 1443–1449 (2018).
- Dohner, E. R., Jaffe, A., Bradshaw, L. R. & Karunadasa, H. I. Intrinsic white-light emission from layered hybrid perovskites. *J. Am. Chem. Soc.* **136**, 13154–13157 (2014).
- Neese, F. The ORCA program system. *Wiley Interdiscip. Rev.: Comput. Mol. Sci.* **2**, 73–78 (2012).
- Neese, F. Software update: the ORCA program system, version 4.0. *Wiley Interdiscip. Rev.: Comput. Mol. Sci.* **8**, e1327 (2018).
- Lu, T. & Chen, F. Multiwfn: A multifunctional wavefunction analyzer. *J. Comput. Chem.* **33**, 580–592 (2012).
- Lin, R. et al. X-ray radiation excited ultralong (>20,000 seconds) intrinsic phosphorescence in aluminum nitride single-crystal scintillators. *Nat. Commun.* **11**, 4351 (2020).
- Bondi, A. van der Waals volumes and radii. *J. Phys. Chem.* **68**, 441–451 (1964).
- Matta, C. F. & Boyd, R. J. An Introduction to the Quantum Theory of Atoms in Molecules. In *The Quantum Theory of Atoms in Molecules* p1–34 (Wiley-VCH Verlag GmbH & Co. KGaA, Weinheim, 2007).
- Wang, Q. et al. Reevaluating protein photoluminescence: remarkable visible luminescence upon concentration and insight into the emission mechanism. *Angew. Chem., Int. Ed.* **58**, 12667–12673 (2019).
- Maldiney, T. et al. The in vivo activation of persistent nanophosphors for optical imaging of vascularization, tumours and grafted cells. *Nat. Mater.* **13**, 418–426 (2014).
- Wu S., Pan Z., Chen R., Liu X. *Long Afterglow Phosphorescent Materials*; Springer.

47. Li, M. et al. Prolonging ultralong organic phosphorescence lifetime to 2.5 s through confining rotation in molecular rotor. *Adv. Opt. Mater.* **7**, 1800820 (2019).
48. Zheng, H. Y., Cao, P. S., Wang, Y. Y., Lu, X. M. & Wu, P. Ultralong room-temperature phosphorescence from boric acid. *Angew. Chem. Int. Ed.* **60**, 9500–9506 (2021).
49. Frisch, M. J. T. et al. Inc., Wallingford CT: 2013.

Acknowledgements

The authors gratefully acknowledge the financial support from the National Natural Science Foundation of China (No. 21522505) and Sichuan Science and Technology Program (No. 2021YFH0124). Detailed characterizations supported by the public Platform of Analytical & Testing Center, Sichuan University, are greatly appreciated.

Author contributions

P.W. supervised this work. P.C. and H.Z. carried out the experimental and theoretical investigations. P.C. and P.W. wrote the manuscript.

Competing interests

The authors declare no competing interests.

Additional information

Supplementary information The online version contains supplementary material available at <https://doi.org/10.1038/s41467-022-33540-1>.

Correspondence and requests for materials should be addressed to Peng Wu.

Peer review information *Nature Communications* thanks the anonymous reviewer(s) for their contribution to the peer review of this work. Peer reviewer reports are available.

Reprints and permission information is available at <http://www.nature.com/reprints>

Publisher's note Springer Nature remains neutral with regard to jurisdictional claims in published maps and institutional affiliations.

Open Access This article is licensed under a Creative Commons Attribution 4.0 International License, which permits use, sharing, adaptation, distribution and reproduction in any medium or format, as long as you give appropriate credit to the original author(s) and the source, provide a link to the Creative Commons license, and indicate if changes were made. The images or other third party material in this article are included in the article's Creative Commons license, unless indicated otherwise in a credit line to the material. If material is not included in the article's Creative Commons license and your intended use is not permitted by statutory regulation or exceeds the permitted use, you will need to obtain permission directly from the copyright holder. To view a copy of this license, visit <http://creativecommons.org/licenses/by/4.0/>.

© The Author(s) 2022